Frontiers in Bioscience Landmark

Front. Biosci. (Landmark Ed) **2026**; 31(6): 49331
https://doi.org/10.31083/FBL49331

Original Research

The Role of Hippocampal Microglial cGAS-STING Signaling Pathway in Postoperative Cognitive Dysfunction in Diabetic Mice

Jiaqi Ning[1,†], Mengjie Chen[1,†], Jiaxi Liu[1], Guanzheng Zhang[1], Siyi Xie[1], Ruyu Yan[1], Yuxuan Yang[1], Zhihao Ren[1], Xiang Li[2], Lingling Ding[1,*], Bin Li[3]

[1]Department of Anesthesiology, Beijing Hospital of Traditional Chinese Medicine, Capital Medical University, 100010 Beijing, China
[2]Department of Acupuncture and Moxibustion, Beijing Pinggu District Hospital of Traditional Chinese Medicine, 101200 Beijing, China
[3]Department of Acupuncture and Moxibustion, Beijing Hospital of Traditional Chinese Medicine, Capital Medical University, 100010 Beijing, China
*Correspondence: dinglingling301@126.com (Lingling Ding)
[†]These authors contributed equally.

Academic Editors: Antoni Camins and Thomas Heinbockel
Submitted: 21 December 2025 Revised: 22 March 2026 Accepted: 22 April 2026 Published: 22 June 2026

Abstract

Objective: This study aimed to determine whether activation of the cyclic GMP-AMP synthase (cGAS)-stimulator of interferon genes (STING) pathway within hippocampal microglia contributes to postoperative cognitive dysfunction (POCD) in a diabetic mouse model. Diabetes was induced using a high-fat, high-sugar (HFHS) diet combined with streptozotocin (STZ). **Methods**: Diabetes was induced in C57BL/6J mice using an HFHS diet followed by STZ. POCD was modeled via tibial fracture surgery under general anesthesia. Cognitive function was assessed using the Open Field Test, Y-maze, and contextual fear conditioning. cGAS-STING pathway activation was evaluated by western blot for cGAS and STING expression. Microglial activation was assessed by co-localization of Iba-1 and CD68 by immunofluorescence, and the co-localization of STING with Iba-1 in the hippocampus was examined by immunofluorescence. Hippocampal neuroinflammation was quantified by enzyme-linked immunosorbent assay (ELISA) for interleukin-1beta (IL-1β) and tumor necrosis factor-alpha (TNF-α). Neuronal injury and apoptosis were evaluated by Nissl staining and western blot for cleaved caspase-3. **Results**: Compared to non-diabetic controls, diabetic mice exhibited cognitive impairments, which were more pronounced in those that underwent surgery. This was accompanied by significant hippocampal neuronal loss, upregulated cleaved caspase-3 expression, and elevated IL-1β and TNF-α levels. Furthermore, diabetic mice that underwent surgery displayed increased expression of microglial activation markers (Iba-1 and CD68) and evidence of cGAS-STING pathway activation in the hippocampus. Immunofluorescence co-localization experiments further suggested a predominant association of this pathway with the microglial marker Iba-1. **Conclusion**: These findings suggest that surgery-associated overactivation of the microglial cGAS-STING pathway in the hippocampus may exacerbate neuroinflammation and neuronal injury, thereby contributing to cognitive decline in diabetic mice.

Keywords: cognitive dysfunction; diabetes mellitus; microglia; cyclic GMP-AMP synthase; STING protein

1. Introduction

Postoperative cognitive dysfunction (POCD) represents one of the most prevalent neurological complications encountered in the surgical setting, manifesting as measurable deterioration across multiple cognitive domains including impairments in learning, memory retention, and sustained attention. Such deficits substantially compromise postoperative recovery trajectories and patients' health-related quality of life, generating considerable socioeconomic costs [1]. Diabetes mellitus (DM) has been widely recognized as an independent risk factor for the development and progression of POCD. Chronic inflammation, oxidative stress, endothelial dysfunction, and central insulin resistance induced by hyperglycemia continuously erode and weaken the brain's defensive and reparative capacities in diabetic patients, establishing a vulnerable pathological state that renders them more susceptible to cognitive impairment when subjected to the acute stress of surgery and anesthesia [2,3].

Among all brain structures, the hippocampus occupies a uniquely vulnerable position owing to its central role in encoding and retrieving declarative memories; its neurons are exquisitely susceptible to ischemic, hypoxic, and inflammatory insults, positioning this region as a primary pathological locus in POCD development [4]. Neuroinflammatory processes are widely regarded as a pivotal mechanistic driver of POCD, with particular clinical relevance in metabolically compromised populations such as diabetic patients [5]. Operative injury provokes both peripheral and central nervous system (CNS) wide inflammatory cascades. In response to this pro-inflammatory milieu, microglia—the resident innate immune sentinels of the CNS—undergo phenotypic transition toward a classically activated (M1) state, characterized by robust secretion of pro-inflammatory mediators including tumor necrosis factor-alpha (TNF-α), interleukin-1beta (IL-1β), and interleukin-6 (IL-6) [6]. This sustained inflammatory signaling compromises blood-brain barrier integrity, perturbs

synaptic transmission, and ultimately precipitates neuronal dysfunction and programmed cell death. In diabetic patients, this pre-existing "pro-inflammatory state" synergistically amplifies with the acute postoperative inflammatory response, exacerbating hippocampal neuroinflammatory damage.

The cyclic GMP-AMP synthase-stimulator of interferon genes (cGAS-STING) signaling axis (comprising cyclic GMP-AMP synthase and its downstream Stimulator of Interferon Genes effector) has emerged as a critically important innate immune surveillance mechanism with growing relevance to neuropathological conditions [7]. Upon encountering cytosolic DNA of exogenous or endogenous origin—including nucleic acids liberated from damaged or dying cells—microglial cGAS is engaged and generates the second messenger cyclic guanosine monophosphate (GMP)-adenosine monophosphate (AMP) (cGAMP). This diffusible molecule subsequently docks onto STING, an adaptor protein anchored to the endoplasmic reticulum membrane, triggering conformational changes that recruit TANK-binding kinase 1 (TBK1) and drive phosphorylation-dependent activation of interferon regulatory factor 3 (IRF3) and nuclear factor kappa B (NF-κB) transcription factors, culminating in the induction of type I interferons and a broad array of pro-inflammatory genes. When chronically engaged under pathological conditions, this signaling cascade sustains deleterious neuroinflammatory states that have been implicated in neurodegenerative processes [8]. Whether surgical stress induces the activation of the cGAS-STING pathway in hippocampal microglia, especially in the context of diabetes, and whether this pathway plays a key role in exacerbating postoperative neuroinflammation and cognitive impairment remain unclear and warrant in-depth investigation.

2. Methods

2.1 Animals and Experimental Design

C57BL/6J mice were used for *in vivo* experiments. All mice were provided by the Laboratory Animal Center of Beijing Hospital of Traditional Chinese Medicine and housed in a specific pathogen-free (SPF) facility at Beijing Hospital of Traditional Chinese Medicine (body weight 18–22 g; temperature 25 ± 2 °C; humidity 50–60%). All researchers received specialized training in laboratory animal operation. Mice were randomly divided into three groups: Control group, Diabetes group, and Diabetes + Surgery group (n = 10 per group). All mice were acclimatized for 1 week before subsequent experiments.

2.2 Establishment of the Diabetic Model

Mice in the Diabetes group were fed a high-fat, high-sugar diet for 8 weeks to establish a metabolic-stress background before streptozotocin (STZ, Sigma, S0130, St. Louis, MO, Germany) induction. After 16 hours of overnight fasting, diabetes model induction was induced by intraperitoneal injection of STZ (70 mg/kg) for three consecutive days. This combined high-fat diet and STZ regimen is a well-established model for type 2 diabetes, as it induces insulin resistance (via diet) and partial β-cell dysfunction (via STZ), closely mimicking human DM pathology [9]. On the 7th day after STZ injection, random blood glucose was measured via tail vein sampling. Mice with random blood glucose >16.7 mmol/L were considered successfully induced. The metabolic characteristics of HFD/STZ-induced diabetic mice are presented in **Supplementary Fig. 1**. Diabetic mice were maintained on a high-fat, high-sugar diet for subsequent studies.

2.3 Establishment of the POCD Model via Tibial Fracture Internal Fixation

Mice in the Diabetes + Surgery group underwent tibial fracture internal fixation to establish the classic POCD model after successful diabetes induction. Induction and maintenance anesthesia were performed using isoflurane (R510-22-2, RWD Life Science, Shenzhen, Guangdong, China). For induction, mice were placed in an induction chamber containing 4% isoflurane until they lost the righting reflex. The mice were then transferred to the surgery table and maintained under anesthesia with a mask delivering a mixture of 1.5% isoflurane and 0.5 L/min O_2. Anesthesia depth was continuously monitored throughout the surgery by checking the absence of the toe pinch reflex. Under sterile surgical conditions, an incision was made on the lateral side of the tibia to expose the bone. A drill hole was created in the tibial plateau for intramedullary nail insertion, followed by osteotomy at the mid-distal tibia, and the incision was sutured continuously. Postoperatively, compound lidocaine cream was applied for analgesia, and mice were placed in clean cages with heat lamp irradiation for rewarming until spontaneous awakening. Mice in the Control and Diabetes groups did not undergo fracture or intramedullary nail insertion, but all other perioperative procedures were consistent with the Diabetes + Surgery group.

2.4 Open Field Test

Each mouse was individually introduced to the center of a square open-field arena (50 × 50 × 40 cm), and automated video tracking (VisuTrack XR-VT101, Shanghai Xinruan Information Technology Co., Ltd, Shanghai, China) was initiated without delay. Exploratory and locomotor behaviors were captured continuously over a 5-minute trial under undisturbed conditions. Primary outcome variables encompassed total locomotion distance, spatial trajectory patterns, and cumulative time spent within the central zone of the arena. Following each trial, the animal was returned to its home cage, and the apparatus surfaces were thoroughly decontaminated with 75% ethanol solution; the subsequent animal's trial commenced only after full environmental equilibration was confirmed, thereby ensuring procedural independence and measurement consistency across animals.

2.5 Y-Maze Test

The Y-maze apparatus featured three equidistant arms arranged at 120° intervals, with individual arm dimensions of 30 × 5 × 15 cm. Animals were placed at the distal end of a randomly selected arm and permitted unrestricted exploration of all three arms for 8 minutes. The order and frequency of arm entries—defined as complete entry of all four paws into an arm—were recorded. The spontaneous alternation rate (SAR) was derived using the following formula: [(number of alternations) / (total arm entries – 2)] × 100%, where an alternation was defined as three consecutive entries into three distinct arms. This index served as a measure of intact hippocampus-dependent spatial working memory.

2.6 Contextual Fear Conditioning Test

Mice were placed in a conditioning chamber (Med Associates) and allowed to acclimatize for 2 minutes, followed by a foot shock (0.7 mA, 2 seconds duration) as the unconditioned stimulus. Immediately after the shock, the mouse was returned to its original cage. Twenty-four hours later, the mouse was reintroduced to the same conditioning chamber for 5 minutes of observation (without shock), and the percentage of freezing time was recorded. Freezing behavior was defined as the absence of any voluntary movement except for breathing, and quantitative analysis was performed using Freeze Frame software (SuperFcs XR-XC404, Shanghai Xinruan, China).

At the designated experimental endpoint, all animals were humanely euthanized via isoflurane overdose. Mice were exposed to 5% isoflurane within the induction chamber until complete loss of consciousness and cessation of spontaneous respiration were verified, whereupon cervical dislocation was immediately performed to confirm death and ensure full compliance with institutional animal welfare guidelines.

2.7 cGAS-STING Pathway Analysis

2.7.1 Western Blot Analysis

Hippocampal tissues were harvested and homogenized in radioimmunoprecipitation assay (RIPA) lysis buffer containing protease and phosphatase inhibitor cocktails on ice to extract total protein. Protein concentration was determined using a bicinchoninic acid (BCA) protein assay kit (Thermo Fisher Scientific, Waltham, MA, USA). Equal amounts of protein (10 µg) were separated by 10% or 12% sodium dodecyl sulfate-polyacrylamide gel electrophoresis (SDS-PAGE) and transferred to polyvinylidene difluoride (PVDF) membranes (Millipore, Burlington, MA, USA). Membranes were blocked with Tris-buffered saline with Tween 20 (TBST) containing 5% non-fat milk for 1 hour at room temperature, followed by incubation with primary antibodies at 4 °C overnight. Primary antibodies included: cGAS (31659S, 1:1000, Cell Signaling Technology, Danvers, MA, USA), phosphorylated STING (72971S, 1:1000, Cell Signaling Technology, USA), phosphorylated TBK1 (5483S, 1:1000, Cell Signaling Technology, USA), phosphorylated IRF3 (29047S, 1:1000, Cell Signaling Technology, USA), and NF-κB p65 (ab16502, 1:1000, Abcam, Cambridge, UK). After washing three times with TBST, membranes were incubated with horseradish peroxidase (HRP)-conjugated secondary antibodies (1:5000, Jackson ImmunoResearch, West Grove, PA, USA) for 1 hour at room temperature. Protein bands were visualized using an enhanced chemiluminescence (ECL) detection kit (34580, Thermo Fisher Scientific), and images were acquired with a ChemiDoc XRS + imaging system (Bio-Rad, Hercules, CA, USA). Band intensities were quantified using ImageJ software (1.54 g, National Institutes of Health, Bethesda, MD, USA), and the expression levels of target proteins were normalized to β-actin (A1978, 1:5000, Sigma-Aldrich, St. Louis, MO, USA) as an internal control.

2.7.2 Immunofluorescence Staining

Coronal cryosections (30 µm) were collected and fixed in 4% paraformaldehyde at 4 °C for 24 hours, followed by permeabilization in phosphate-buffered saline (PBS) supplemented with 0.3% Triton X-100 (15 minutes) and blocking in PBS containing 5% bovine serum albumin (BSA) for 1 hour at room temperature. Sections were then co-incubated overnight at 4 °C with paired primary antibodies: Iba-1 (microglial marker, 1:500, Wako, Richmond, VA, USA) combined with either CD68 (activated microglial marker, 1:500, Abcam) or STING (1:500, Cell Signaling Technology). Following three washes in PBS, sections were exposed to Alexa Fluor 488- or 594-conjugated secondary antibodies (1:1000, Thermo Fisher Scientific) for 1 hour at room temperature protected from light. Nuclei were counterstained with 4′,6-diamidino-2-phenylindole (DAPI). Images were captured using a confocal microscope, and the co-localization of Iba-1 with CD68 or STING was analyzed using ZEISS software (ZEISS ZEN 3.13, Oberkochen, Germany).

2.7.3 Enzyme-Linked Immunosorbent Assay (ELISA)

Hippocampal tissue homogenates were prepared in ice-cold PBS containing protease inhibitors, clarified by centrifugation at 12,000 ×g for 15 minutes at 4 °C, and supernatants were retained for cytokine quantification. Concentrations of IL-1β and TNF-α were determined using validated commercial ELISA kits (MLB00C, MTA00B, R&D Systems, R&D Systems, Minneapolis, MN, USA) in strict accordance with the supplier's protocols. Brief steps: Standards and samples (100 µL/well) were added to antibody-precoated 96-well plates and incubated at 37 °C for 2 hours; after washing, detection antibodies (100 µL/well) were added and incubated at 37 °C for 1 hour; substrate solution (100 µL/well) was then added and incubated at 37 °C for 30 minutes; the reaction was terminated by adding stop

solution, and absorbance was measured at 450 nm using a microplate reader (SYNERGY H1, BioTek, Winooski, VT, USA). Cytokine concentrations in samples were calculated based on serial dilution standard curves of recombinant IL-1β and TNF-α.

2.8 Neuronal Damage Detection

2.8.1 Nissl Staining

Paraffin-embedded brain sections underwent sequential deparaffinization in xylene and graded rehydration through an ethanol series (100%, 95%, 80%, and 70%), after which they were stained with 0.1% cresyl violet acetate at 37 °C for 10 minutes. Sections were differentiated with 95% ethanol for 30 seconds, dehydrated with absolute ethanol, cleared with xylene, and mounted with neutral balsam. Neuronal morphology was observed under a light microscope (Olympus BX53, Olympus Corporation, Tokyo, Japan), and the number of intact neurons (defined as neurons with clear nuclei and Nissl bodies) was counted in designated brain regions (e.g., hippocampal CA1 area). Three sections per mouse and three non-overlapping fields per section were selected for quantitative analysis using ImageJ (Version 1.53g, National Institutes of Health, Bethesda, MD, USA) software.

2.8.2 Western Blot Analysis for cleaved caspase-3

Total protein extraction from brain tissues was performed as described in the "western blot" section. The level of neuronal apoptosis was detected using an antibody against cleaved caspase-3 (9661S, 1:1000, Cell Signaling Technology, USA). Band intensities were quantified with ImageJ software, normalized to β-actin as an internal control, and the relative expression level of cleaved caspase-3 was calculated.

2.9 Statistical Analysis

All statistical analyses were performed using GraphPad Prism 9.0 (GraphPad Software, Boston, MA, USA) and SPSS 22.0 (IBM, Armonk, NY, USA). Normality of distributions was assessed using the Shapiro–Wilk test; when relevant, variance homogeneity was evaluated using Levene's test. Data passing normality (and homogeneity where applicable) are presented as mean ± SD and were compared among multiple groups using one-way analysis of variance (ANOVA) followed by Tukey's post-hoc test. Data failing normality are presented as median (interquartile range, IQR) and were compared using the Kruskal–Wallis test followed by Dunn's post-hoc test with Bonferroni correction. All statistical tests were two-tailed, and $p < 0.05$ was considered statistically significant. Sample sizes were chosen consistent with commonly used group sizes in comparable behavioral and neuroinflammation mouse studies and considering ethical/practical constraints; future confirmatory studies should incorporate prospective power calculations.

3. Results

3.1 Cognitive Function Assessment of Mice in the Three Groups

Cognitive function was evaluated from three dimensions (spontaneous activity, spatial learning and memory, and associative learning and memory) using the Open Field Test, Y-Maze Test, and Contextual Fear Conditioning Test (Fig. 1). Results showed significant differences in cognitive function among the three groups ($p < 0.05$). The combination of the Y-maze, Open Field Test, and Fear Conditioning Test covers both "hippocampus-dependent memory (FC)" and "working memory (Y-maze)", while using the Open Field Test, to quantify locomotion and anxiety. This approach significantly reduces the misinterpretation of false-positive cognitive differences caused by physical or motor limitations in fracture models. Compared to high motor-load tasks (such as the Morris water maze), it is better suited for the early postoperative window in a tibial fracture internal fixation model of POCD.

The Open Field Test revealed no significant difference in total distance traveled among the three groups ($p > 0.05$), suggesting no obvious differences in gross locomotor activity, thereby reducing the likelihood that motor impairment confounded subsequent cognitive assessments. Regarding time spent in the central zone (commonly interpreted as an anxiety-like behavior index), compared with the Control group, the Diabetes group showed a significantly shorter central-zone residence time ($p < 0.05$); the Diabetes + Surgery group exhibited a further significant reduction compared with the Diabetes group ($p < 0.05$), indicating increased anxiety in diabetic mice that was exacerbated by surgery.

In the Y-Maze Test, the spatial alternation rate was (68.2 ± 4.5)% in the Control group, (52.1 ± 3.8)% in the Diabetes group (significantly lower than the Control group, $p < 0.05$), and (39.5 ± 4.2)% in the Diabetes + Surgery group (significantly lower than the Diabetes group, $p < 0.05$). These results indicated that diabetes impairs spatial learning and memory in mice, and tibial fracture surgery further exacerbates this cognitive deficit.

In the Contextual Fear Conditioning Test, during the context test, the percentage of freezing time was (67.9 ± 5.1)% in the Control group, (45.4 ± 5.0)% in the Diabetes group ($p < 0.05$ vs. Control group), and (28.6 ± 4.3)% in the Diabetes + Surgery group ($p < 0.05$ vs. Diabetes group). During the cue test, a similar trend was observed: (61.0 ± 4.8)% in the Control group, (42.8 ± 4.7)% in the Diabetes group ($p < 0.05$ vs. Control group), and (26.3 ± 3.9)% in the Diabetes + Surgery group ($p < 0.05$ vs. Diabetes group). These results suggested that diabetic mice have impaired associative learning and memory, and surgical trauma significantly aggravates this cognitive impairment.

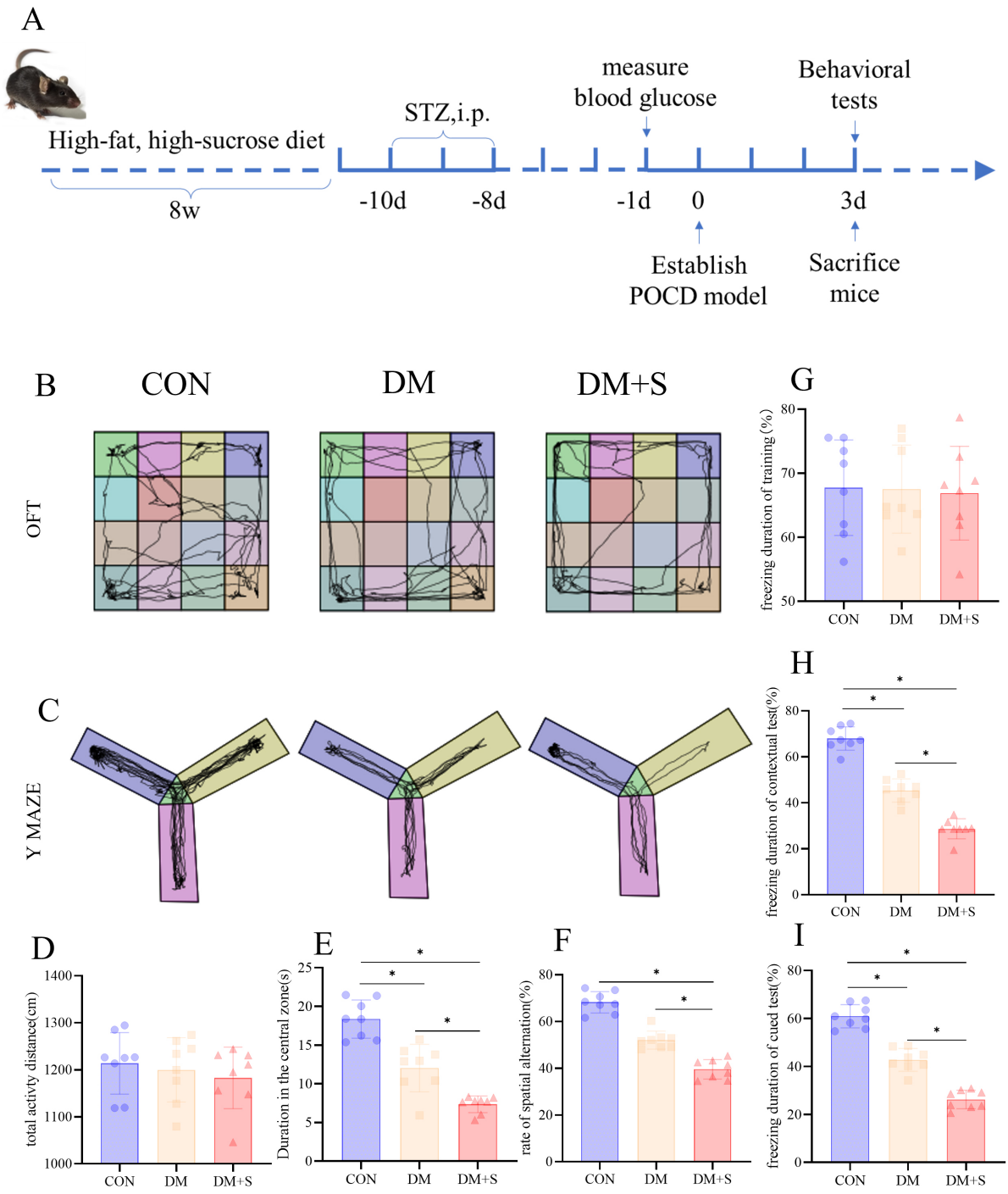

Fig. 1. Impaired postoperative cognitive function in diabetic postoperative cognitive dysfunction (POCD) mice. (A) Experimental flowchart. (B) Representative movement traces in the open field test. (C) Representative arm entry sequences in the Y-maze test. (D) Total distance traveled in the open field test (no significant differences). (E) Time spent in the central zone of the open field, showing decreased time in diabetic groups, indicating increased anxiety. (F) Spontaneous alternation rate in the Y-maze test, showing impaired spatial working memory in diabetic groups. (G) Freezing time during training phase of fear conditioning (no differences). (H) Freezing time in context test, showing impaired contextual memory. (I) Freezing time in cued test, showing impaired cued memory. Data are mean ± SD. *$p < 0.05$. STZ, streptozotocin; i.p., intraperitoneal injection; CON, control group; DM, diabetes mellitus group; S, surgery; DM+S, diabetes mellitus + surgery group; OFT, open field test; FC, fear conditioning; w, week(s); d, day(s).

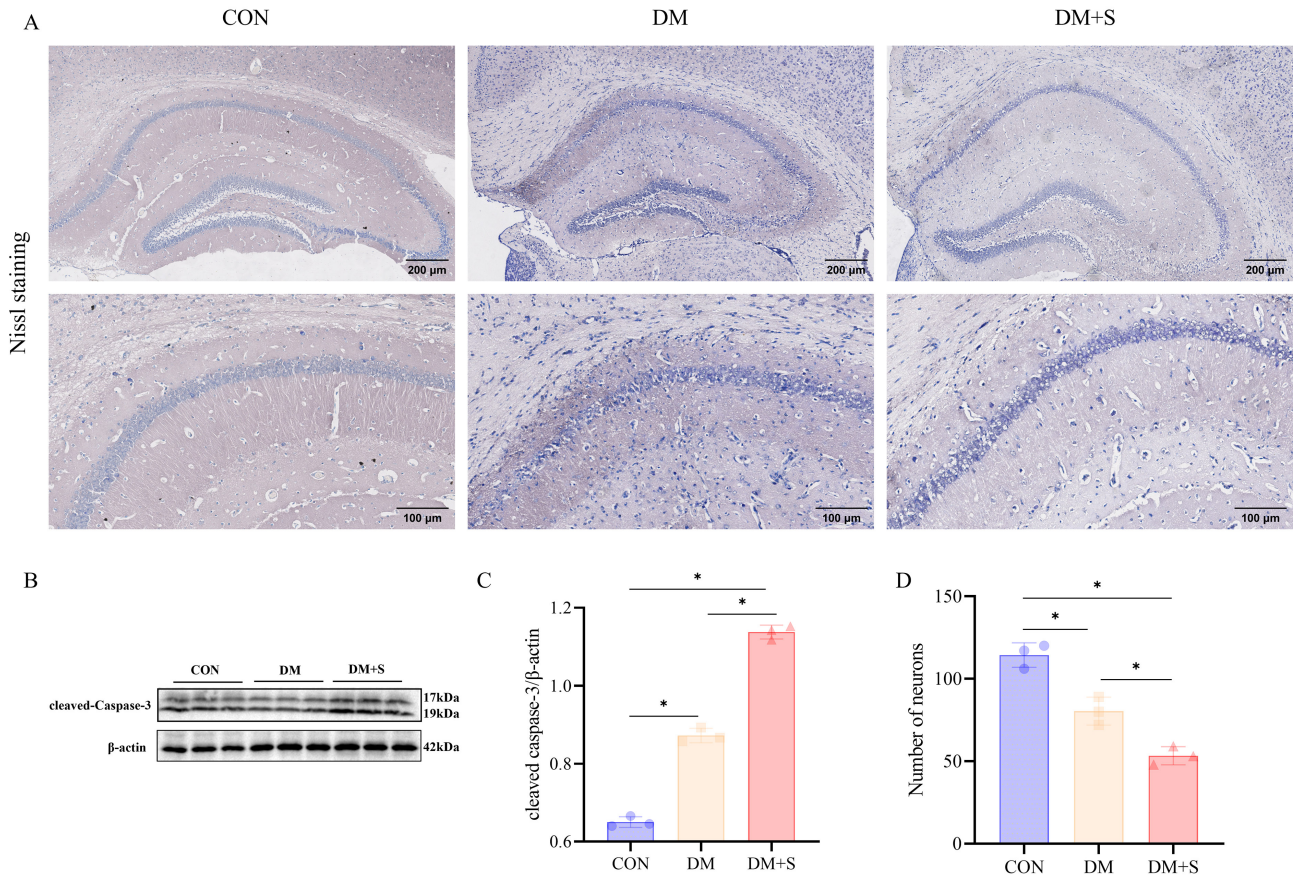

Fig. 2. Neuronal injury and cleaved caspase-3 expression in the hippocampus of diabetic POCD mice. (A,D) Representative Nissl staining images of the hippocampal CA1 region showing neuronal loss. Upper row Scale bars = 200 μm; lower row Scale bars = 100 μm. (B,C) Western blot analysis of cleaved caspase-3 expression, showing increased apoptosis in diabetic and surgical groups. Data are mean ± SD. *$p < 0.05$. POCD, postoperative cognitive dysfunction; CA1, cornu ammonis 1; CON, control group; DM, diabetes mellitus group; S, surgery; DM+S, diabetes mellitus + surgery group.

3.2 Hippocampal Neuronal Injury and cleaved caspase-3 expression

Nissl staining was used to assess hippocampal neuronal loss and Western blot for cleaved caspase-3 was used to assess hippocampal neuronal apoptosis, and significant differences were observed among the three groups.

Nissl staining showed that neurons in the hippocampus (CA1 region shown) of the Control group were neatly arranged, dense, with plump cell bodies and abundant Nissl bodies. In the Diabetes group, hippocampal neurons were disorganized, significantly reduced in number compared with the Control group ($p < 0.05$), with some neuronal somata atrophied and Nissl bodies decreased. The Diabetes + Surgery group exhibited more severe hippocampal neuronal damage: the number of neurons was further reduced compared with the Diabetes group ($p < 0.05$), with massive disintegration of neuronal somata and almost complete loss of Nissl bodies (Fig. 2A,D).

Western blot results showed that the expression level of the apoptotic key protein cleaved caspase-3 in the hippocampus was significantly higher in the Diabetes group than in the Control group ($p < 0.05$), and was further significantly upregulated in the Diabetes + Surgery group compared with the Diabetes group ($p < 0.05$). These results indicated that diabetes induces hippocampal neuronal apoptosis, and surgical trauma significantly exacerbates the degree of neuronal apoptosis in diabetic mice (Fig. 2B,C).

3.3 Microglial Activation in the Hippocampus of Three Groups

Immunofluorescence staining was used to observe the morphology and distribution of microglia, evaluating hippocampal microglial activation in the three groups (Fig. 3).

Immunofluorescence results showed that microglia in the hippocampus of the Control group were in a resting state, characterized by small cell bodies, slender and dense branches, and uniform distribution, with minimal co-localization signals of Iba-1 and CD68. In the Diabetes group, hippocampal microglia had enlarged cell bodies and shortened, thickened branches, showing partial activation characteristics, with increased co-localization signals of Iba-1 and CD68. In the Diabetes + Surgery group,

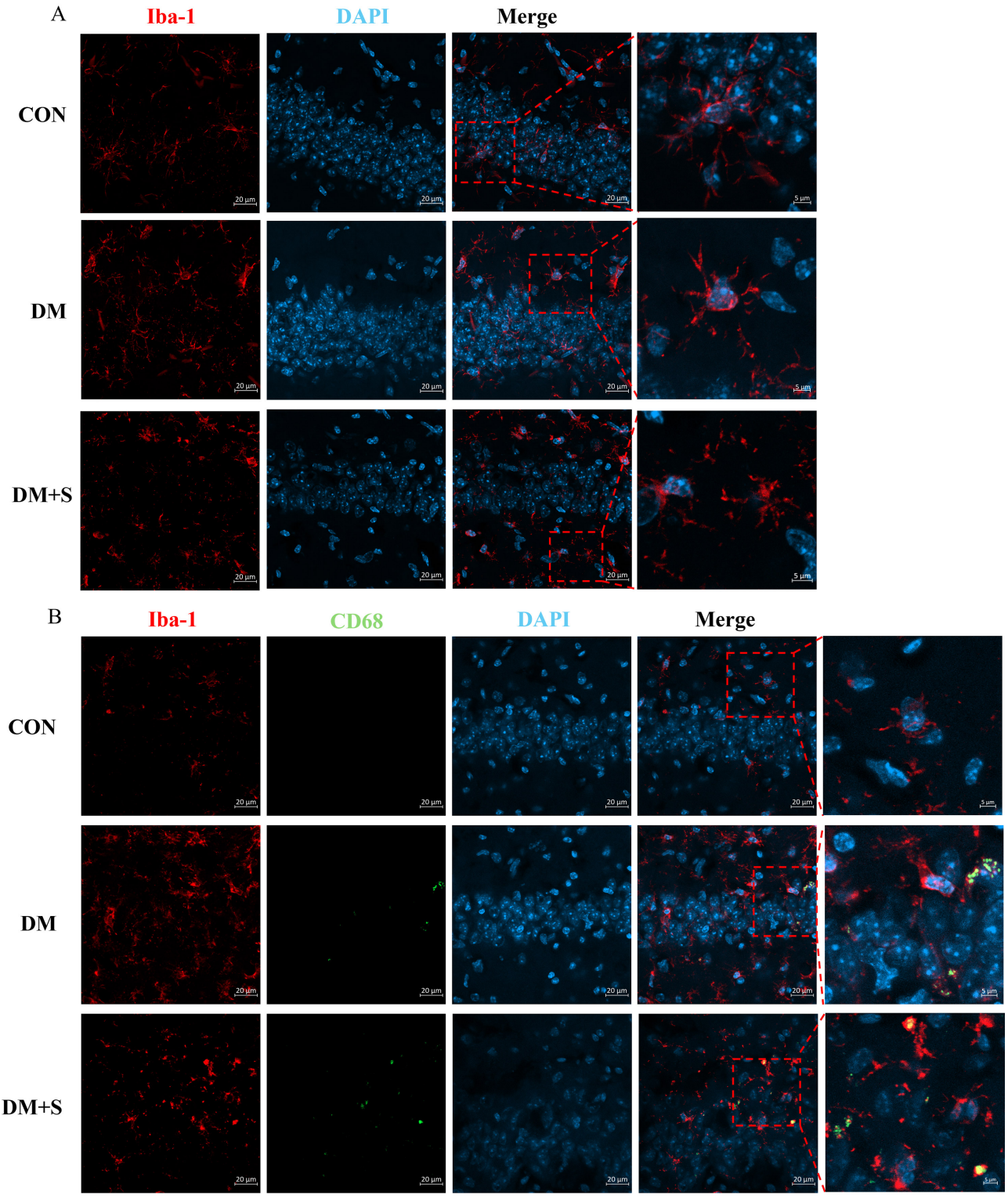

Fig. 3. Microglial activation in the hippocampus of three groups of mice. (A) Immunofluorescence staining for Iba-1 (red) showing morphological changes in microglia. (B) Co-localization of Iba-1 (red) and CD68 (green) indicating activated microglia; increased co-localization in diabetic and surgical groups. Iba-1, ionized calcium-binding adapter molecule 1; CD68, cluster of differentiation 68; DAPI, 4′,6-diamidino-2-phenylindole; CON, control group; DM, diabetes mellitus group; S, surgery; DM+S, diabetes mellitus + surgery group. Scale bars, 20 μm (main image) and 5 μm (inset).

hippocampal microglia were fully activated, presenting a typical amoeboid morphology with significantly enlarged cell bodies, almost complete loss of branches, and significantly increased cell density; the co-localization signals of

Iba-1 and CD68 were significantly enhanced. These results indicated that diabetes induces microglial activation and polarization toward the pro-inflammatory phenotype, and surgical trauma significantly exacerbates this activation and polarization process (Fig. 3).

3.4 Activation of the cGAS-STING Pathway and Its Colocalization With Microglia in the Hippocampus

To clarify the role of the cGAS-STING pathway in POCD of diabetic mice, Western blot was used to detect the expression levels of key pathway molecules (cGAS and STING), and immunofluorescence double-labeling was performed to observe the co-localization of STING with the microglial marker Iba-1.

Western blot results showed low expression levels of cGAS and p-STING proteins in the hippocampus of the Control group, indicating a quiescent state of the pathway. In the Diabetes group, the expression levels of cGAS and p-STING proteins were significantly higher than those in the Control group ($p < 0.05$), accompanied by marked upregulation of the downstream signaling molecules p-TBK1 and p-IRF3, as well as NF-κB p65 protein levels ($p < 0.05$), suggesting partial activation of the pathway and its downstream inflammatory signaling in the hippocampus. Furthermore, compared with the Diabetes group, the Diabetes + Surgery group showed further significant increases in cGAS, p-STING, p-TBK1, p-IRF3, and NF-κB p65 protein levels ($p < 0.05$). These findings indicate that surgical trauma further exacerbates diabetes-induced activation of the hippocampal cGAS–STING pathway, as reflected by enhanced STING, TBK1, and IRF3 phosphorylation and increased NF-κB p65 expression (Fig. 4A–F).

Immunofluorescence double-labeling results showed minimal STING-positive signals in the hippocampus of the Control group, with little co-localization with Iba-1-positive microglia. In the Diabetes group, STING-positive signals were increased, and some STING-positive signals colocalized with Iba-1-positive microglia. In the Diabetes + Surgery group, STING-positive signals were substantially increased and showed predominant co-localization with Iba-1-positive microglia, particularly in morphologically activated microglia. These observations suggest that the cGAS-STING pathway is activated in the hippocampus of diabetic mice after surgery, with signals largely associated with microglia in our imaging; however, rigorous cell-type attribution would benefit from quantitative co-localization metrics and additional cell markers in future studies (Fig. 4G).

3.5 Expression Levels of Neuroinflammatory Cytokines in the Hippocampus

ELISA was used to detect the expression levels of pro-inflammatory cytokines (IL-1β and TNF-α) in the hippocampus, evaluating neuroinflammatory responses mediated by microglial activation and cGAS-STING pathway activation. Results showed low levels of IL-1β and TNF-α in the hippocampus of the Control group. In the Diabetes group, the levels of IL-1β and TNF-α were significantly higher than those in the Control group ($p < 0.05$). In the Diabetes + Surgery group, the levels of IL-1β and TNF-α were further significantly upregulated compared with the Diabetes group ($p < 0.05$). These results indicated that diabetes induces chronic low-grade neuroinflammation in the hippocampus, and surgical trauma significantly exacerbates this neuroinflammatory response, consistent with the trends of microglial activation and cGAS-STING pathway activation (Fig. 4H,I).

4. Discussion

POCD constitutes a clinically significant postoperative neurological sequela, predominantly manifesting as deterioration in learning and memory capacities along with attentional deficits that substantially diminish patients' quality of life following surgical procedures. Accumulating evidence from recent investigations establishes diabetes as an independent risk determinant for POCD, with affected individuals demonstrating a markedly elevated incidence compared to metabolically healthy surgical cohorts [3], but the specific mechanism remains incompletely elucidated. This study found that diabetic mice already exhibited cognitive impairment without surgical intervention, accompanied by increased hippocampal neuronal apoptosis and elevated expression of pro-inflammatory factors such as IL-1β and TNF-α, which is consistent with previous research results. The hippocampus is a key brain region for learning and memory, and the integrity of its neurons directly determines cognitive function. Under diabetes conditions, sustained hyperglycemia, insulin resistance, and oxidative stress can induce hippocampal neuronal apoptosis, while activating microglia to trigger chronic neuroinflammation [10]; these two processes jointly contribute to baseline cognitive impairment.

As a core inducer of POCD, surgical trauma can exacerbate CNS damage through multiple pathways such as peripheral inflammatory cascades, oxidative stress, and blood-brain barrier disruption [11]. This study showed that cognitive impairment, neuronal apoptosis, and neuroinflammation in the Diabetes + Surgery group were significantly more severe than those in the Diabetes group, suggesting that the "baseline inflammatory microenvironment" under diabetic conditions can amplify the central damage induced by surgical trauma. This finding further validates the "two-hit" hypothesis: the underlying CNS lesions caused by diabetes represent the "first hit", and surgical trauma serves as the "second hit"; their synergistic effect promotes the development and progression of POCD.

As the resident macrophages and primary immunosurveillance cells of the CNS, microglia are indispensable guardians of central neural homeostasis [12], adopting a highly ramified, surveilling morphology under basal condi-

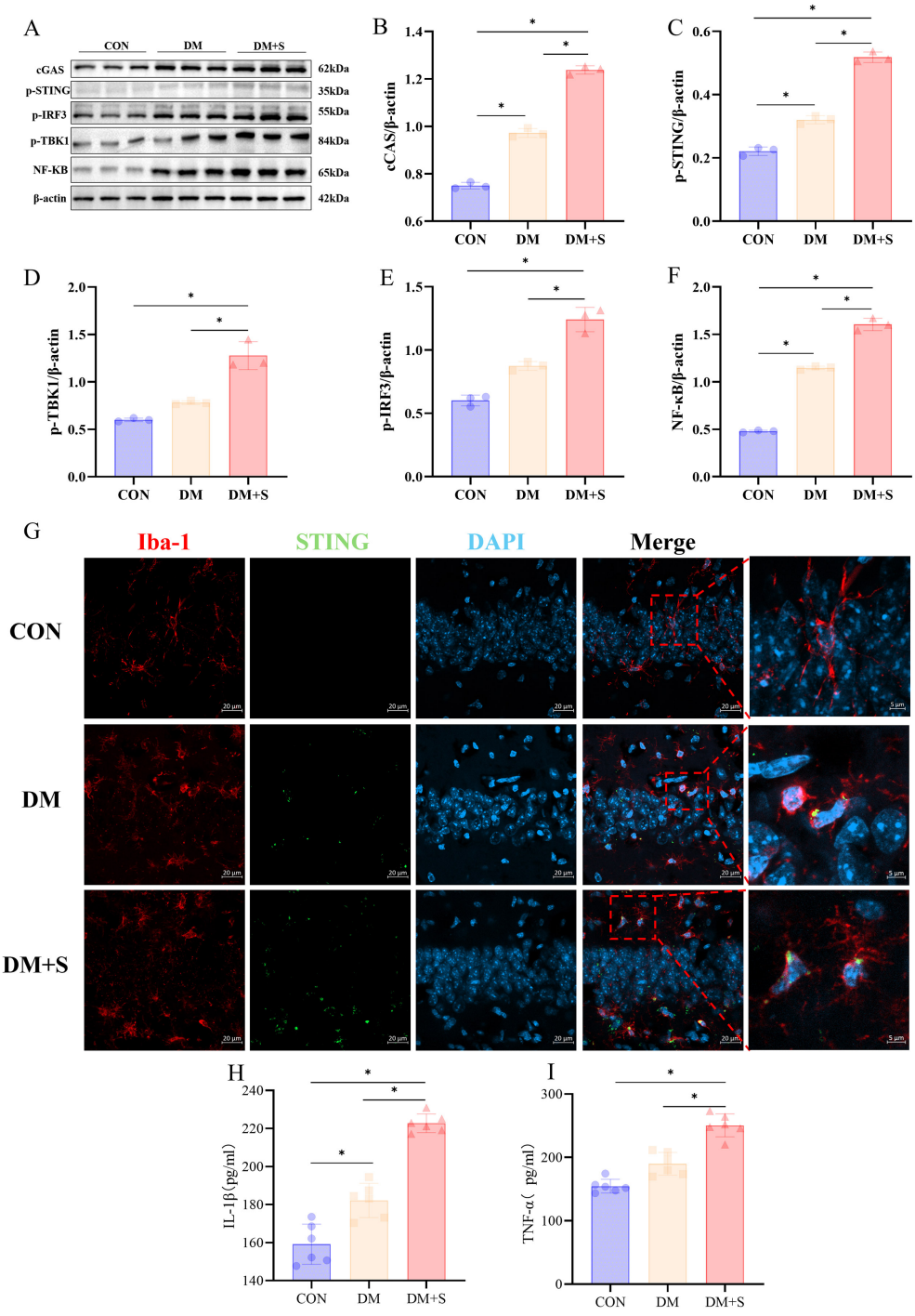

Fig. 4. Activation of the cGAS-STING pathway in the hippocampus of mice and its co-localization with microglia. (A–F) Western blot analysis of cGAS, p-STING, p-TBK1, p-IRF3, and NF-κB p65 expression, showing increased pathway activation in diabetic and surgical groups. (G) Immunofluorescence co-localization of STING (green) with Iba-1 (red) in the hippocampus. (H,I) Enzyme-linked immunosorbent assay (ELISA) results for interleukin-1beta (IL-1β) and tumor necrosis factor-alpha (TNF-α), showing increased pro-inflammatory cytokines in diabetic and surgical groups. Data are mean ± SD. *$p < 0.05$. cGAS, cyclic GMP-AMP synthase; STING, stimulator of interferon genes; p-, phosphorylated; TBK1, TANK-binding kinase 1; IRF3, interferon regulatory factor 3; NF-κB, nuclear factor kappa B; Iba-1, ionized calcium-binding adapter molecule 1; DAPI, 4′,6-diamidino-2-phenylindole; CON, control group; DM, diabetes mellitus group; S, surgery; DM+S, diabetes mellitus + surgery group. Scale bars, 20 μm (main image) and 5 μm (inset).

tions while actively participating in essential maintenance functions including synaptic remodeling, debris clearance, and modulation of neurotransmitter homeostasis. When stimulated by pathological factors, microglia can activate and differentiate into the pro-inflammatory M1 phenotype. M1-type microglia can release pro-inflammatory factors such as IL-1β and TNF-α, exacerbating neuroinflammation and inducing neuronal apoptosis [10]. In this study, the expression levels of Iba-1 and CD68 (M1-type markers) in the hippocampus of the Diabetes group were significantly increased, and microglia showed a partially activated morphology. In the Diabetes + Surgery group, hippocampal microglia were fully activated into an amoeboid shape, CD68 expression was further significantly increased, accompanied by a significant increase in pro-inflammatory factors (IL-1β and TNF-α) and a significant aggravation of neuronal apoptosis. These results suggest that diabetes is associated with polarization of microglia toward a pro-inflammatory (M1-like) phenotype, and surgical trauma can significantly enhance this polarization process. Activated microglia mediate neuroinflammation by releasing large amounts of pro-inflammatory factors, thereby being linked to neuronal injury and cognitive impairment. Previous studies have suggested the key role of microglial activation in POCD [6], and this study further clarified the specificity of microglial activation under diabetic conditions: chronic hyperglycemia and insulin resistance induced by diabetes lead to sustained microglial activation, forming "inflammatory memory". When stimulated by surgical trauma, microglia with "inflammatory memory" can produce a stronger pro-inflammatory response, thereby exacerbating neural damage. This mechanism may be an important reason for the increased susceptibility to POCD in patients with diabetes.

The cGAS-STING pathway constitutes a key cytoplasmic DNA-sensing mechanism that has emerged as a central regulator of innate immune responses. When cells are subjected to stimuli such as damage or infection, abnormal DNA (e.g., pathogen-derived DNA, self-DNA released from damaged cells) can appear in the cytoplasm. cGAS can recognize this abnormal DNA and catalyze the production of cyclic GMP-AMP (cGAMP). cGAMP binds to and activates p-STING, which recruits downstream kinase p-TBK1 to further activate downstream signaling pathways such as p-IRF3 and NF-κB, inducing the expression of pro-inflammatory factors. Recent studies have suggested that the cGAS-STING pathway plays an important role in CNS diseases such as neurodegenerative diseases and brain injury [7,8], but its role in diabetes-related POCD has not been reported. In this study, the expression levels of cGAS and p-STING proteins in the hippocampus of the Diabetes group were significantly increased, indicating baseline activation of the pathway. In the Diabetes + Surgery group, the expression levels of cGAS and p-STING proteins were further significantly upregulated, and immunofluorescence double-labeling suggested that p-STING was mainly colocalized with the microglial marker Iba-1, especially in activated amoeboid microglia. Combined with our findings on microglial activation and neuroinflammation, we propose the following mechanism: under diabetic conditions, hippocampal neurons may undergo chronic injury and release self-derived DNA. This aberrant DNA could be engulfed by microglia and translocated into the cytoplasm, thereby activating the cGAS–STING pathway and promoting microglial polarization toward an M1-like pro-inflammatory phenotype. Surgical trauma may induce more extensive neuronal damage and further increase the release of self-DNA, leading to additional activation of the microglial cGAS–STING pathway. This, in turn, amplifies microglial activation and the production of pro-inflammatory mediators, establishing a self-reinforcing pathogenic loop in which DNA release triggers cGAS–STING signaling, intensifies microglial activation and neuroinflammation, and ultimately aggravates neuronal injury and cognitive decline. Whereas previous studies have largely emphasized inflammatory pathways such as Toll-like receptor 4 (TLR4) and NOD-like receptor family pyrin domain containing 3 (NLRP3) in POCD [13], our data highlight a central contribution of the cytosolic DNA-sensing cGAS–STING axis to diabetes-associated POCD. These findings offer a complementary mechanistic framework and may help explain the heightened vulnerability to POCD observed in patients with diabetes.

Interestingly, the cGAS-STING pathway may interact with other well-established inflammatory pathways in POCD. For instance, STING activation can prime the NLRP3 inflammasome via NF-κB signaling, leading to enhanced IL-1β production [14,15]. Additionally, mitochondrial DNA release, a common trigger for both cGAS-STING and Toll-like receptor 9 (TLR9) pathways, could serve as a unifying mechanism linking these responses [16]. In the diabetic hippocampus, chronic inflammation may sensitize microglia to surgical stress, resulting in synergistic activation of multiple pathways and amplifying neuroinflammation. Future studies should explore these potential interactions to fully elucidate the complex inflammatory network underlying POCD in diabetes.

This study has several limitations. First, we did not perform specific inhibition or genetic knockdown of the cGAS-STING pathway, so the causal relationship between pathway activation and cognitive decline remains to be established. Future studies using pharmacological inhibitors (e.g., C-176, H-151) or conditional knockout mice are needed to confirm the mechanistic role of this pathway. Second, we did not measure plasma insulin levels or perform pancreatic histology to validate the DM phenotype; however, the high-fat diet/STZ model is widely accepted as a DM model [9]. Third, we did not assess astrocyte activation (astrogliosis), which is another important component of neuroinflammation; future investigations should in-

clude markers such as glial fibrillary acidic protein (GFAP). Fourth, we did not explore the upstream triggers of cGAS-STING activation, such as the source of cytosolic DNA (e.g., mitochondrial DNA or nuclear DNA). Finally, this is an animal study, and the findings require validation in clinical samples. Despite these limitations, our study provides the first evidence linking the cGAS-STING pathway to POCD in the context of diabetes.

5. Conclusion

This study showed that diabetic mice exhibited baseline cognitive impairment, and surgical trauma further exacerbated this deficit. Activation of the cGAS-STING pathway in hippocampal microglia was associated with microglial pro-inflammatory activation, increased neuroinflammation, and enhanced neuronal injury in the diabetic surgical context, which may contribute to POCD-like behaviors. These findings provide a perspective for understanding the increased susceptibility to postoperative neurocognitive impairment in diabetes and suggest the cGAS-STING axis as a potential target that warrants causal validation in future inhibition/knockout studies.

Availability of Data and Materials

The datasets generated and analyzed during the current study are available from the corresponding author on reasonable request.

Author Contributions

JN and MC contributed equally to this work (co-first authors). They designed the research framework, performed the main experiments, analyzed the experimental data, and drafted the initial manuscript. JL, GZ, SX, RY, YY and ZR participated in the experimental operation, assisted with data collection and sorting, and provided constructive suggestions for the manuscript revision. XL and BL offered theoretical guidance for the research, participated in the discussion of research results, and revised the manuscript critically for important intellectual content. LD (corresponding author) conceived and supervised the entire research project, finalized the manuscript, and was responsible for the overall integrity and scientific validity of the work. She also handled the submission and revision process of the manuscript. All authors contributed to editorial changes in the manuscript. All authors read and approved the final manuscript. All authors have participated sufficiently in the work and agreed to be accountable for all aspects of the work.

Ethics Approval and Consent to Participate

All experimental procedures adhered to the Guidelines for the Ethical Review of Laboratory Animal Welfare (GB/T 35892-2018) and the Guide for the Care and Use of Laboratory Animals (8th edition, NIH). The study was carried out in accordance with the ARRIVE guidelines. The protocol was approved by the Experimental Animal Ethics Committee of Beijing Hospital of Traditional Chinese Medicine (approval no. BJTCM-M-2025-10-04).

Acknowledgment

Not applicable.

Funding

This work was supported by National Natural Science Foundation of China (82374580); 2024 Beijing Science and Technology Plan "AI+Health Collaborative Innovation Cultivation" Special Project: Research and Development and Demonstration Application of Digital Therapy Products for Cognitive Impairment Diseases (Project No.: Z241100007724008).

Conflicts of Interest

The authors declare no conflicts of interest.

Declaration of AI and AI-Assisted Technologies in the Writing Process

AI-assisted tools (ChatGPT 5.5 and DeepSeek-V3) were used solely for language translation and linguistic refinement to improve the clarity and readability of the manuscript. These tools did not contribute to the generation of scientific ideas, research content, data analysis, image creation, or any experimental or computational procedures. All study design, data collection, data interpretation, and scientific conclusions were completed entirely by the authors.

Supplementary Material

Supplementary material associated with this article can be found, in the online version, at https://doi.org/10.31083/FBL49331.

References

[1] Lin X, Luo Y, Zhu Q. Postoperative cognitive dysfunction and neurodegeneration: From inflammation to precision medicine. Brain Research Bulletin. 2026; 237: 111776. https://doi.org/10.1016/j.brainresbull.2026.111776

[2] Liu H, Chen J, Ling J, Wu Y, Yang P, Liu X, et al. The association between diabetes mellitus and postoperative cognitive dysfunction: a systematic review and meta-analysis. International Journal of Surgery (London, England). 2025; 111: 2633–2650. https://doi.org/10.1097/JS9.0000000000002156

[3] Li H, Xue J, Gao Z, Xian L, Yuan J, He J. Diabetes mellitus is associated with an increased risk of postoperative neurocognitive disorders: a systematic review. Frontiers in Medicine. 2026; 13: 1726908. https://doi.org/10.3389/fmed.2026.1726908

[4] Hu L, Liu SP, Sun J, Sun Z, Song L, Liu C, et al. Impact of surgical interventions on postoperative cognitive dysfunction: A focus on gene expression in the hippocampus and cerebral cortex and peripheral blood cells. Experimental Neurology. 2025; 394: 115459. https://doi.org/10.1016/j.expneurol.2025.115459

[5] Jiao XH, Wan J, Wu WF, Ma LH, Chen C, Dong W, et al.

GLT-1 downregulation in hippocampal astrocytes induced by type 2 diabetes contributes to postoperative cognitive dysfunction in adult mice. CNS Neuroscience & Therapeutics. 2024; 30: e70024. https://doi.org/10.1111/cns.70024

[6] Wu X, He T, He F, Liu L. Is postoperative cognitive dysfunction a disease of microglial inflammatory memory? A state-transition model from metabolic stress to epigenetic lock-in. Frontiers in Molecular Neuroscience. 2025; 18: 1648161. https://doi.org/10.3389/fnmol.2025.1648161

[7] Gulen MF, Samson N, Keller A, Schwabenland M, Liu C, Glück S, et al. cGAS-STING drives ageing-related inflammation and neurodegeneration. Nature. 2023; 620: 374–380. https://doi.org/10.1038/s41586-023-06373-1

[8] Decout A, Katz JD, Venkatraman S, Ablasser A. The cGAS-STING pathway as a therapeutic target in inflammatory diseases. Nature Reviews. Immunology. 2021; 21: 548–569. https://doi.org/10.1038/s41577-021-00524-z

[9] Brito AKDS, Mendes AVDS, Timah Acha B, Santos Oliveira ASDS, Lopes Macedo J, Suzuki Cruzio A, et al. Experimental Models of Type 2 Diabetes Mellitus Induced by Combining Hyperlipidemic Diet (HFD) and Streptozotocin Administration in Rats: An Integrative Review. Biomedicines. 2025; 13: 1158. https://doi.org/10.3390/biomedicines13051158

[10] Tian Y, Jing G, Ma M, Yin R, Zhang M. Microglial activation and polarization in type 2 diabetes-related cognitive impairment: A focused review of pathogenesis. Neuroscience and Biobehavioral Reviews. 2024; 165: 105848. https://doi.org/10.1016/j.neubiorev.2024.105848

[11] Ying C, Lin F. The Role of Immune Cell Subsets in the Development of Postoperative Cognitive Dysfunction in Surgical Patients under Anesthesia. Neuroimmunomodulation. 2025; 32: 306–321. https://doi.org/10.1159/000548491

[12] Nayak D, Roth TL, McGavern DB. Microglia development and function. Annual Review of Immunology. 2014; 32: 367–402. https://doi.org/10.1146/annurev-immunol-032713-120240

[13] Wang T, Sun G, Tao B. Updated insights into the NLRP3 inflammasome in postoperative cognitive dysfunction: emerging mechanisms and treatments. Frontiers in Aging Neuroscience. 2024; 16: 1480502. https://doi.org/10.3389/fnagi.2024.1480502

[14] Chen KQ, Tang WR, Liu X. Research and progress of cGAS/STING/NLRP3 signaling pathway: a mini review. Frontiers in Immunology. 2025; 16: 1594133. https://doi.org/10.3389/fimmu.2025.1594133

[15] Li H, Wang X, Luo X, Shi H, Li J. cGAS/STING/NLRP3 Signaling Pathway-Mediated Pyroptosis in Hypertrophic Cardiomyopathy Radiotherapy. Frontiers in Bioscience (Landmark Edition). 2025; 30: 26084. https://doi.org/10.31083/FBL26084

[16] Tao G, Liao W, Hou J, Jiang X, Deng X, Chen G, et al. Advances in crosstalk among innate immune pathways activated by mitochondrial DNA. Heliyon. 2024; 10: e24029. https://doi.org/10.1016/j.heliyon.2024.e24029